Testing the Vogt-Bailey Index using task-based fMRI across pulse sequence protocols

Kristian Galea[1], Aitor Alberdi Escudero[2], Nina Attard-Montalto[2], Nolan Vella[3], Robert E. Smith[4, 5], Christine Farrugia[6], Paola Galdi[7], Kenneth Scerri[8], Liam Butler[2], and Claude J. Bajada[1,2,9,*]

[1]The University of Malta, University of Malta Magnetic Resonance Imaging Platform, Msida, MSD2080, Malta
[2]The University of Malta, Department of Physiology and Biochemistry, Msida, MSD2080, Malta
[3]Mater Dei Hospital, Medical Physics Department of Medical Imaging, Msida, MSD2090, Malta
[4]The University of Melbourne, Florey Department of Neuroscience and Mental Health, Victoria, Australia
[5]The University of Melbourne, Florey Institute of Neuroscience and Mental Health, Victoria, Australia
[6]The University of Edinburgh, Centre for Clinical Brain Sciences, Edinburgh, EH16 4SB, Scotland
[7]The University of Edinburgh, School of Informatics, Edinburgh, EH89AB, Scotland
[8]The University of Malta, Faculty of Engineering, Msida, MSD2080, Malta
[9]The University of Malta, Faculty of Media & Knowledge Sciences, Msida, MSD2080, Malta
[*]claude.bajada@um.edu.mt

ABSTRACT

Local connectivity analyses in fMRI such as the Vogt-Bailey Index, investigate the prevalence of co-fluctuations in the time-series of adjacent voxels. While there have been *in silico* assessments of the VB Index, this technique has not yet been assessed *in vivo*. This study has two aims: first, to assess the VB Index using a task paradigm with well established *a priori* expectations on the brain region predominantly responsible for executing this task to determine whether the VB Index highlights this area. Second, we investigate if, and how, the spatial resolution of the sequence protocols employed, with their inherent effects on the signal-to-noise ratio, affect the resultant VB maps. A cohort of 10 research volunteers underwent fMRI acquisitions utilising a block design finger tapping experiment. Each volunteer was scanned with three sequence protocols, with all parameters equivalent except for the volume of the voxels. The resulting parametric maps derived using the VB Index were compared with those obtained from the conventional General Linear Model approach. Particular emphasis was placed on the identification of the hand portion of the motor homunculus. Across sequence protocols, the VB Index consistently identified elevated local connectivity in, qualitatively, the same portion of the motor cortex as that yielded by the General Linear Model based on the task paradigm. However, the VB Index also detected elevated local connectivity outside the motor cortex while the General Linear Model results were mostly restricted to the motor cortex. The consistently high VB Index, across sequence protocols, in the cortical region associated with an fMRI task paradigm, despite the approach's agnosticism to that task, provides support for the biological relevance of such local connectivity measures.

Introduction

A subset of the various data analysis methods employed in functional Magnetic Resonance Imaging (fMRI) are local connectivity methods. These data analysis methods are predicated on the assumption that the voxels encompassed by a brain region with elevated neural activity are temporally similar to each other, reflecting the underlying synchronous neural activity[1,2]. Therefore, local connectivity methods infer brain function by assessing the similarity between the time-series signal of local voxel neighbourhoods.

One such local connectivity measure of relevance to this work is the VB Index[3], a technique that employs a searchlight approach to iteratively assess local connectivity. For each voxel, the algorithm formulates a graph with adjacent voxels within that neighbourhood as vertices and the modified Pearson correlation coefficient between their respective fMRI time series as the edge weights. The VB Index is derived from the eigenvalue decomposition of the Laplacian matrix of that graph. This metric is normalised to the range 0.0-1.0, with higher values indicating stronger correlation within the local neighbourhood; more specifically, the higher the VB Index, the less readily can the graph be disconnected into two parts (as such, the VB Index behaves somewhat as an edge detection technique)[3,4].

A desirable attribute of local connectivity methods is that they do not require explicit prior knowledge on what the participant is doing, cognitively while they are lying in the scanner. This makes local connectivity methods particularly suited for resting-state fMRI data analysis where prior knowledge may not be readily available[1]. However, an inherent challenge with

resting-state fMRI analysis is the lack of readily available "ground truth". Thus, assessing local connectivity methods *in vivo*, particularly in resting-state fMRI is challenging.

One possible way to perform *in vivo* assessment of local connectivity methods would be to evaluate their outcomes in an experiment where activity of a known brain region is explicitly evoked and verifiable using alternative analysis techniques. This is the definition of task-based fMRI, where there is a rich history of task paradigms and association of brain regions to such[5–8]. Typically, in task-based fMRI, each image voxel is analysed using the General Linear Model (GLM)[9], which models the voxels time-series signal as a weighted sum of regressors, including the Blood Oxygenation Level Dependent (BOLD) signal predicted by explicit engagement and disengagement with the task. Statistical tests are then applied to identify voxels with a time-series that exhibits a significant fit to the model[10–12]. Any meaningful local connectivity algorithm should ideally exhibit elevated values in the brain regions with association with the task performed. Although such assessment has been previously performed for an earlier local connectivity measure, Regional Homogeneity (ReHo)[13,14], the VB Index has thus far only been validated using synthetic data[4].

Therefore, this study aims to provide an *in vivo* assessment of the VB Index using such a well-established task. We investigate whether the VB Index identifies the primary region of interest for an associated task. Specifically, in this study, the task performed is that of finger tapping, and the associated primary region of interest is the motor cortex. To provide a reference map for this assessment, we employ a standard GLM analysis on the same data.

Given the mechanism by which the VB Index is calculated, it was hypothesized that the spatial resolution of the fMRI acquisition may have a considerable impact on its ability to identify task-related activation where the functional region is physically small. For conventional GLM analysis, it is only necessary to measure at least one image voxel with a time series correlated with the task. With adequate signal-to-noise ratio (SNR), the model will suitably associate that voxel with the task. Further, fMRI data are typically smoothed prior to model fitting, sacrificing spatial specificity for sensitivity to the effect. For the VB Index to become elevated however requires that multiple adjacent image voxels co-fluctuate with one another, hence only being sensitive to functional regions that encompass multiple image voxels. Relatedly, larger voxels and hence poorer resolution may encompass an entire functionally-homogeneous region within a single voxel, rendering the VB index ineffective at detecting local connectivity. Yet if the spatial resolution is too high the sensitivity of the VB Index to that co-fluctuation may be corrupted by low SNR[15]. Further, performing smoothing of fMRI data is expected *a priori* to artificially elevate the VB Index everywhere given that it would explicitly impose co-fluctuations in adjacent voxels. Given these confounds, our investigation of the VB Index was performed at multiple acquisition resolutions, and with two alternative strategies for data smoothing.

Results

Three separate analysis pipelines were run on the preprocessed fMRI data; two different pipelines of the VB Index, and a classical GLM analysis. The first VB approach (hereafter VB1) replicated the smoothing operation commonly adopted for conventional GLM analysis, where the fMRI data are spatially smoothed prior to model fitting to increase the SNR. The second VB approach (hereafter VB2) involved the application of spatial smoothing after the VB analysis. In VB2 smoothing was carried out to account for residual misalignment in functional localisation relative to anatomy. Further, the order of smoothing for VB2 conformed with the standard VB Index pipeline of computing the metric on unsmoothed data. Given that the VB Index is an edge-detection technique sensitive to functional boundaries[4], it was hypothesized that operating on unsmoothed data would better localise the contrast of functional boundaries.

GLM results

Slices from the second-level GLM statistical maps obtained for each sequence protocol are given in Figure 1. Activation was detected consistently across sequence protocols in the precentral gyrus of the motor cortex, an Omega shaped region in the axial plane, commonly referred to as the "hand knob" region. Furthermore, activity was detected consistently in the occipital lobe, clearly seen from the right sagittal slices in Figures 1a, 1b and 1c.

VB Index results

Figures 2 and 3 show slices from the resulting statistical maps obtained using VB1 and VB2 respectively. In both VB pipelines, significantly high VB values were found consistently across sequence protocols in the precentral gyrus of the motor cortex in agreement with the GLM (Figure 1). Furthermore, significantly high VB values were also detected in the occipital lobe across sequence protocols in both VB methods, as seen by the right sagittal slices of Figures 2a, 2b, 2c (VB1) and 3a, 3b, 3c (VB2). In contrast to the results from the GLM, significantly high VB Index values (Figures 2 and 3) were not limited to the motor cortex or the occipital lobe, but included other brain regions including the thalamus, supplementary motor area, premotor area, and the parietal lobe. Across the two VB pipelines the maps exhibit qualitatively similar significant regions. However, the areas of significant coherence identified in the VB1 method (Figure 2) where smoothing was applied to the fMRI data prior to VB

computation were more diffused when compared to the VB2 method where smoothing was applied to the VB Index maps after VB computation (Figure 3).

Quantitative analysis

Given that the same task paradigm was performed by the volunteers for each sequence, it was hypothesised that the results acquired with the three sequence protocols would be consistent. Therefore, the consistency of the statistical maps across resolutions was assessed using the Dice coefficient (Figure 4). Following the nomenclature of Wilson et al., (2017)[16], the spatial similarity between pairs of statistical maps which depends on the magnitude of the Dice coefficient shall be described as being; low if the similarity metric ranges from 0.00 to 0.19, low-moderate; 0.20 to 0.39, moderate: 0.40 to 0.59, moderate-high; 0.60 to 0.79 or high; 0.80 to 1.00. The results obtained with the GLM exhibited the highest overall consistency across pulse sequences (Figure 4a), with moderately-high Dice coefficients ranging from 0.616 to 0.687. VB1 maps had the second-highest consistency across pulse sequences, as seen in Figure 4b, with moderate Dice coefficients ranging from 0.497 to 0.566. The VB2 maps were the least consistent across sequences (Figure 4c), with low-moderate Dice coefficients ranging from 0.354 to 0.372.

In order to assess the VB Index, the resulting VB maps obtained with both VB pipelines were compared to those of the GLM, a standard technique in fMRI analysis[10]. The Overlap coefficient was used to quantify the fraction of the GLM significant result also identified using the VB Index (Figure 5). The nomenclature of Wilson et al., (2017)[16] shall also be used to describe the overlap of pairs of statistical maps. VB1 exhibited the highest overlap with the GLM results, as seen in Figure 5a, with moderate to moderately-high Overlap coefficients ranging from 0.4 to 0.7. Conversely, VB2 exhibited less overlap with the GLM, as seen in Figure 5b, with low to moderate Overlap coefficients ranging from 0.1 to 0.4.

Discussion

The lack of available ground truth in resting-state fMRI analysis makes it inherently difficult to assess local connectivity approaches. Though the VB Index was previously tested with synthetic data[4], it had not yet been tested on empirical fMRI data. Therefore, the study aimed to use a well established task-based experimental paradigm with a well known pattern of expected activity to assess the VB Index and its ability to detect and characterise the task-related activity. Further, this assessment was carried out across sequence protocols with differing spatial resolutions and two different smoothing strategies to investigate their impact on the VB Index's results. Results demonstrated that the VB Index reliably identifies known task-related activations across resolutions, with clear qualitative overlap with statistical maps generated by the GLM. While the GLM analysis highlighted activations conforming to the predefined task model, primarily in the motor and visual cortices, the VB Index indicated elevated local connectivity in a broader set of regions. These additional regions may reflect either alternate neuronal activity present during the experiment which may or may not have been directly caused by the execution of the motor task or are a result of artifactual correlations within the data.

The GLM analysis, based on the predefined task model, revealed significant activation in the left motor cortex, contralateral to the hand used in the task, consistent with previous research[5–8]. Activity was detected consistently in the precentral gyrus which is heavily involved in hand motor function[17], and in the occipital lobe (Figures 1) which is primarily responsible for visual perception[18]. Given that visual stimulus presentation differed subtly during task and rest conditions (central white fixation cross versus laterised coloured targets shown to the participants during the experiment), some activity in the occipital region was expected.

The data were analysed using the VB Index with two separate approaches. In both VB pipelines, clusters of significantly high local connectivity were identified across sequences in the precentral gyrus (Figures 2 and 3 for VB1 and VB2, respectively). The elevated local connectivity detected in the precentral gyrus with VB1 approach largely overlapped with the area identified by the GLM, while the elevated local connectivity detected in the same area with VB2 was more spatially refined, delineating a smaller region within the precentral gyrus. Both VB pipelines revealed elevated local connectivity in the occipital lobe across sequences, as seen in the right sagittal slices in Figures 2 and 3. VB2 identified more localised regions of elevated local connectivity in both the precentral gyrus and the occipital lobe (see supplementary material), compared to both GLM and VB1, indicating the method's sensitivity to finer-scale variations in local connectivity. Furthermore, task-related activity within the cerebellum, in line with literature[5,7], was detected by the GLM, but only for the 2.5^3 mm^3 acquisition; both VB pipelines identified elevated local connectivity at the same location, though similarly only for the 2.5^3 mm^3 acquisition. This provides some limited additional support for VB being sensitive to genuine localised neuronal activity.

Compared to VB1, VB2 results were generally less diffused (see Figures 2, 3, and supplementary material). Furthermore, higher resolution sequence protocols, when analysed with VB2, yielded more spatially specific patterns. This is possibly because unsmoothed higher resolution data inherently contains finer spatial details[19], allowing for a more precise presentation of local connectivity. The finer spatial detail revealed by VB2, particularly at higher resolutions, aligns with areas from previous research demonstrating somatotopic organisation within the motor cortex during finger movements[20–22]. Conversely, VB1, by

applying smoothing before the VB analysis, activation patterns were more diffused, potentially obscuring finer-scale variations in local connectivity. These findings suggest that VB1 may be preferred when a broader overview of local connectivity is desired, while VB2 is better suited for investigating finer spatial variations, particularly when using higher resolution data.

The findings demonstrate that the VB Index can consistently detect elevated local connectivity in brain regions with anticipated elevated task-related neural activity. This partially validates the VB Index's sensitivity to coherency in the BOLD signal in empirical data. Although outside the scope of the study, the results indicate that due to the ability of the VB index to highlight the expected task-related brain regions, apart from its use in resting-state fMRI studies, may also be used as an alternate analysis technique for task-based fMRI studies.

The Dice coefficient was used for the pairwise comparison of the statistical maps generated by the different analysis methods across sequence protocols. This analysis revealed varying degrees of consistency. The GLM results showed the highest consistency, followed by VB1, with VB2 exhibiting the lowest consistency across sequences. A certain degree of consistency was indeed expected across sequences as participants were subjected to the same tasks and fixed real space distance smoothing for each sequence protocol. However, perfect congruence was not anticipated due to differences in the SNR across sequences, and inherent variability in task performance which could have contributed to differences between runs.

The Overlap coefficient was used to assess the spatial intersection of the VB and the GLM (Figure 5) with the GLM statistical map as reference. VB1 showed greater spatial overlap with the GLM compared to VB2, which possibly reflects the finer spatial detail captured by VB2, which may not always align perfectly across subjects. The VB results obtained with the lowest resolution (2.5^3 mm^3) sequence protocol had, overall, the highest spatial overlap with any of the three GLM maps.

While the results obtained with lower resolutions had higher spatial overlaps with the GLM with smoother and more diffused activation patterns, such lower resolutions may not well capture spatially small activations. Therefore, the spatial resolution should be sufficiently high to sample an activated functional area ensuring that a voxel's neighborhood encompasses a functionally homogeneous region. However, increasing spatial resolution comes at the cost of reduced SNR which could consequently degrade the sensitivity of VB Index to the BOLD signal. Therefore, optimising data acquisition for the purpose of VB analysis involves a trade-off between the competing demands of spatial resolution and SNR.

Future work to our study may focus on addressing both the limited number of participants and test paradigms used. Nevertheless, the robust nature of the expected activation patterns associated with this simple motor task was determined to provide adequate statistical power for this preliminary validation study, despite the relatively small sample size. Further work could also focus on the development of test paradigms specific for the use of local connectivity analysis for task-based fMRI data.

This study demonstrated that the VB Index was able to detect and characterise task-related brain activity across pulse sequence protocols (different spatial resolutions). The VB Index reliably identified elevated local connectivity in key regions associated with a finger-tapping task, including the motor cortex and occipital lobe, with results that qualitatively overlapped with those of a conventional GLM analysis. Pre-smoothing the fMRI data prior to VB Index quantification (VB1) resulted in broad patterns of significantly elevated local connectivity, moderate overlap with GLM results, and reasonable consistency across sequence protocols; conversely, application to unsmoothed data (VB2) revealed fine spatial details of significantly elevated local connectivity that align with known somatotopic organisation in the motor cortex, particularly at higher acquisition resolutions, though with reduced consistency across protocols. These findings highlight the VB Index's sensitivity to local BOLD signal coherence and serve as preliminary validation of the VB Index. Thus, they provide evidence of its' sensitivity to known biological effects and support its' application in resting state fMRI analysis. Finally, while more investigation is needed, it also suggests that the VB Index may have some utility in analysing task-based data.

Methods

Participants

Ten research volunteers (aged 22 to 55 years; mean±standard deviation 31.5±10.4 years) were recruited for the study. Nine of the volunteers were male and one was female. Seven of the volunteers were right-handed. Prior to the MRI scanning, written informed consent was obtained from the participants. In order to be eligible to participate, the volunteers had to have normal or corrected-to-normal vision. The study was granted ethics approval by the Faculty of Health Science Research Ethics Committee (FREC) at the University of Malta.

Scanning protocols

A SIEMENS 3T MAGNETOM Vida (Siemens Healthcare GmbH, Erlangen, Germany) MRI system was used throughout. The BioMatrix Head/Neck 64 channel coil (Siemens Healthcare GmbH, Erlangen, Germany) was used for reception of the radiofrequency signal during the MRI scanning. The volunteers were positioned in a supine position on the MRI gantry, with their head at the centre of the head coil. Each volunteer was scanned for a period of approximately one hour.

Each volunteer was scanned using a high-resolution T1-weighted MPRAGE axial pulse sequence (1^3 mm^3 isotropic voxels, TE=2.66ms, TR=2190ms, TI=925ms, flip angle=8°, GRAPPA; R=2). Then, a gradient field map image was acquired (2.5^3 mm^3 isotropic voxels, TR=529ms, TE_1=4.92ms, TE_2=7.38ms, flip angle=60°). Eight of the ten volunteers were scanned with a high-resolution T2-weighted SPACE axial sequence (1^3 mm^3 isotropic voxels, TE=417ms, TR=3140ms, variable flip angle, GRAPPA; R=2, turbo factor = 282).

The volunteers were scanned using three different gradient echo planar imaging (EPI) pulse sequences. The three EPI sequences, referred to as the 2.5^3 mm^3 , 2.0^3 mm^3 and 1.8^3 mm^3 sequences, employed consistent scanning parameters (flip angle=65°, TR=1840ms, TE=34ms, simultaneous multi slice (SMS) with a multiband factor (MB) of 4, phase partial Fourier of 6/8) except for the volume of the voxels which was set to 2.5^3 mm^3 (field of view (FOV)=240×240mm^2, in-plane resolution=96×96, Bandwidth=2084Hz/Px), 2^3mm^3 (FOV=240×240mm^2, in-plane resolution=120×120, Bandwidth=2084Hz/Px), or 1.8^3 mm^3 (FOV=241×241 mm^2 , in-plane resolution=134×134, Bandwidth=2072Hz/Px). For each EPI sequence, a total of 60 axial slices (with no slice gaps) and 393 volumes were acquired, with an acquisition time of approximately 12 minutes. The order in which the different sequences were acquired for each participant was shuffled.

fMRI experimental paradigm

Participants were required to complete a finger tapping task while being scanned with the three EPI sequences. The task required participants to tap either their right thumb or index finger at the onset of a particular visual stimulus. This was done using the NordicNeuroLab response grip (NordicNeuroLab AS, Bergen, Norway). The experimental task was explained to participants before scanning commenced.

The experimental finger tapping task was designed using PsychoPy[23]. The task instructions were synchronised with the fMRI volume acquisition using the NordicNeuroLab SyncBox (NordicNeuroLab AS, Bergen, Norway). The times at which the buttons were pressed and the times at which the fMRI volumes were acquired were stored.

The task included three visual stimuli, a white fixation cross shown during rest periods at the centre of the screen, and the active stimuli were presented as coloured crosses on the right side of the screen, with a red cross corresponding to tapping of the right thumb and blue cross corresponding to tapping of the right index finger. All three stimuli were presented on a solid grey background. Participants were instructed to tap their right thumb at the onset of the red cross, and to tap their right index finger at the onset of the blue cross. Participants were required to repeatedly tap either the thumb or the index finger until the end of each trial, at which point the white fixation cross was presented, upon which they were instructed to rest and stop tapping their thumb/finger. Each experimental trial lasted about 18.4s (10 fMRI volumes), and was followed by a rest period of equal length. For each block within the set of experimental trials, the tapping finger (thumb or index) was chosen at random, but the overall structure of alternating task (tapping) and rest periods remained consistent throughout the scan.

Data pre-processing

The MRI data were first structured according to the brain imaging data structure (BIDS) standard[24] using the "BIDSKIT" tool (`https://github.com/jmtyszka/bidskit`). fMRIPrep (version 23.2.0)[25,26] was then used to preprocess the structural and functional data. The recommended fMRIPrep boilerplate text is reproduced verbatim in the next few subsections except for minor adjustments for formatting, language, and clarity.

Preprocessing of B_0 inhomogeneity mappings

A total of 10 fieldmaps were found available within the input BIDS structure. Then, for each volunteer, a B0 nonuniformity map (or fieldmap) was estimated from the phase-drift maps measured with two consecutive gradient-recalled echo (GRE) acquisitions. The corresponding phase-maps were phase-unwrapped with 'prelude' (FSL version 6.0[27–29]).

Anatomical data preprocessing

A total of 10 T1-weighted (T1w) images were available within the input BIDS dataset. Each T1w image was corrected for intensity non-uniformity (INU) with 'N4BiasFieldCorrection'[30], distributed with ANTs 2.5.0[31], and used as T1w-reference throughout the workflow. The T1w-reference was then skull-stripped with a Nipype implementation of the 'antsBrainExtraction.sh' workflow (from ANTs), using OASIS30ANTs as target template. Brain tissue segmentation of cerebrospinal fluid (CSF), white-matter (WM) and gray-matter (GM) was performed on the brain-extracted T1w using 'fast' [FSL (version 6.0),[27–29]]. Brain surfaces were reconstructed using 'recon-all' [FreeSurfer 7.3.2,[32]], and the brain mask estimated previously was refined with a custom variation of the method to reconcile ANTs-derived and FreeSurfer-derived segmentations of the cortical gray-matter of Mindboggle[33].

Where a T2-weighted image was available, it was used to improve pial surface refinement. Brain surfaces were reconstructed using 'recon-all' [FreeSurfer 7.3.2,[32], and the brain mask estimated previously was refined with a custom variation of the method to reconcile ANTs-derived and FreeSurfer-derived segmentations of the cortical gray-matter of Mindboggle[33]. Volume-based spatial normalisation to one standard space (MNI152NLin2009cAsym) was performed through nonlinear registration

with ‘antsRegistration‘ (ANTs 2.5.0,[31,34]), using brain-extracted versions of both T1w reference and the T1w template. The following template was selected for spatial normalization and accessed with TemplateFlow [23.1.0,[35]: ICBM 152 Nonlinear Asymmetrical template version 2009c [[36,37]; TemplateFlow ID: MNI152NLin2009cAsym].

Functional data preprocessing

For each of the 3 BOLD runs found per subject, the following preprocessing was performed. First, a reference volume was generated, using a custom methodology of fMRIPrep, for use in head motion correction. Head-motion parameters with respect to the BOLD reference (as rigid-body transformation matrices) were estimated using ‘mcflirt‘ [FSL 6.0,[38]] before any spatiotemporal filtering. The estimated fieldmap was then aligned with rigid-registration to the target EPI (echo-planar imaging) reference run. The field coefficients were mapped to the reference EPI using the transform. The BOLD reference was then co-registered to the T1w reference using ‘bbregister‘ (FreeSurfer) which implements boundary-based registration[39]. Co-registration was configured with six degrees of freedom. Several confounding time-series were calculated based on the preprocessed BOLD: framewise displacement (FD), framewise displacement and the derivative of the root mean squared variance over voxels (DVARS), and three region-wise global signals. FD was computed using two formulations following Power et al., (2012) (absolute sum of relative motions,[40]) and Jenkinson et al., (2012)[38] (relative root mean square displacement between affines). FD and DVARS were calculated for each functional run, both using their implementations in Nipype [following the definitions by Power et al., (2012)[40]]. Three global signals were extracted within the CSF, the WM, and the whole-brain masks. Additionally, a set of physiological regressors were extracted to allow for component-based noise correction [CompCor,[41]]. Principal components were estimated after high-pass filtering the preprocessed BOLD time-series (using a discrete cosine filter with 128s cut-off) for the two CompCor variants: temporal (tCompCor) and anatomical (aCompCor). tCompCor components were then calculated from the top 2% variable voxels within the brain mask. For aCompCor, three probabilistic masks (CSF, WM and combined CSF+WM) were generated in anatomical space. The implementation differs from that of Behzadi et al., (2007)[41] in that instead of eroding the masks by 2 pixels in BOLD space, a mask of pixels that likely contain a volume fraction of GM is subtracted from the aCompCor masks. This mask is obtained by dilating a GM mask extracted from FreeSurfer's aseg segmentation, and it ensures components are not extracted from voxels containing a minimal fraction of GM. Finally, these masks were resampled into BOLD space and binarized by thresholding at 0.99 (as in the original implementation). Components were calculated separately within the WM and CSF masks. For each CompCor decomposition, the k components with the largest singular values were retained, such that the retained components' time-series were sufficient to explain 50 percent of variance across the nuisance mask (CSF, WM, combined, or temporal). The remaining components were dropped from consideration. The head-motion estimates calculated in the correction step were also placed within the corresponding confounds file. The confound time-series derived from head motion estimates and global signals were expanded with the inclusion of temporal derivatives and quadratic terms for each 38. Frames that exceeded a threshold of 0.5 mm FD or 1.5 standardized DVARS were annotated as motion outliers. Additional nuisance time-series were calculated by means of principal component analysis of the signal found within a thin band (crown) of voxels around the edge of the brain[42]. All resamplings were performed with a single interpolation step by composing all the pertinent transformations (i.e. head-motion transform matrices, susceptibility distortion correction when available, and co-registrations to anatomical and output spaces). Gridded (volumetric) resamplings were performed using ‘nitransforms‘, configured with cubic B-spline interpolation.

Many internal operations of fMRIPrep use Nilearn 0.10.2 [`http://nilearn.github.io/`], mostly within the functional processing workflow. For more details of the pipeline, see the section corresponding to workflows in fMRIPrep's documentation (`https://fmriprep.readthedocs.io/en/latest/workflows.html`).

Data analysis

General Linear Model Analysis

The preprocessed fMRI data for each volunteer acquired with each EPI sequence was using the GLM. The GLM was constructed using the Python library Nilearn (version 0.10.3). The GLM analysis consisted of a first-level GLM computed for each subject separately, and a second-level GLM which provided statistical inferences at a group level.

Prior to the first-level statistical testing, the fMRI data of each subject were spatially smoothed to improve the SNR and account for inter-subject anatomical variability[43]. A Gaussian kernel with a full width at half maximum (FWHM) of 4.806 mm was selected based on the recommendations of Weibull et al., (2008)[19] for voxels of volume 1.8^3 mm^3. To ensure consistency, the same FWHM was applied for all image series regardless of acquired resolution.

Three mass-univariate first-level GLMs were fit to the smoothed data from each volunteer (one per sequence protocol). For each first-level GLM, the design matrix contained two experimental regressors that modelled the BOLD signal response during the task period (task regressor), and during the rest period (rest regressor). The experimental regressors were modelled as the convolution of the Glover Haemodynamic Response Function (HRF)[44] and the stimulus function of the experiment. In this case, the stimulus function had a duration equivalent to one stimulus period, i.e., 10 fMRI volumes; 10×1.84=18.4s. The timings of the on-off period used to construct the boxcar stimulus function were acquired from the NordicNeuroLab system. The design

matrices also contained a number of confound regressors, extracted by fMRIPrep, that modelled various nuisance parameters including 24 motion-related regressors. A total of 10 discrete cosine transform regressors generated by fMRIPrep were also included in the design matrix to model low-frequency physiological and scanner noise. The first 6 principal components, extracted by fMRIPrep using principal component analysis (PCA) on regions of interest identified by the anatomical CompCor method as being unlikely to be modulated by neural activity[26,41] were also included in the design matrix for each participant. Finally, the global signal regressor was also included in the design matrix since it were shown to improve confound regression performance when used with CompCor[45]. Outlier fMRI volumes containing sudden and large motion artefacts were scrubbed from the GLM analysis, by applying thresholds to the DVARS determined by fMRIPrep for each fMRI volume in each run. Thresholds of 0.5 mm for the FD[46], and 2 for the standardised DVARS[40] were chosen.

The GLM model was then fit to the spatially smoothed fMRI data for each volunteer and sequence separately. A one-sided one-sample t-test was applied to assess differences between task and rest.

The MNI152NLin2009cAsym T1-weighted image with a resolution of 2.0^3 mm^3 was chosen as the primary common template, which was then downsampled to 3.0^3 mm^3 resolution (such that transforming processed data to template space would involve downsampling only) using trilinear interpolation with FSL[27]. The resulting statistical maps were spatially normalised to the template image during the preprocessing stage using the ANTs library[34].

A second-level GLM analysis was performed per acquisition resolution for group-level inferences using a mass-univariate one-sample t-test on the spatially normalised statistical maps. An alpha level of 0.05 was selected, and the Bonferroni correction method was applied to control the familywise error rate (FWE) and threshold the group-level statistical maps. The thresholded group-level statistical maps will be referred to hereafter as statistical maps.

The Vogt-Bailey Index

While the GLM permits addition of confounding signals to the model itself for regression of their explanatory power, calculation of the VB Index offers no such mechanism. Therefore, prior to the VB analysis, a denoising pipeline based on the work of Satterthwaite et al., (2013)[46] was applied to the fMRI data using the rsDenoise library[47] (`https://github.com/adolphslab/rsDenoise.git`).

The preprocessed and denoised fMRI data were analysed with the VB Index in two separate pipelines. The VB method 1 (VB1) replicated the smoothing operation performed during the GLM analysis for fair comparison. Therefore, in VB1 the denoised fMRI data were first smoothed with a Gaussian FWHM of 4.806 mm prior to the computation of the volumetric VB Index. In the VB method 2 (VB2), the volumetric VB Index was computed from the denoised data, and the resulting VB Index maps were spatially smoothed to ensure informative group-level results by accounting for residual inter-subject anatomical variability. The VB Index maps resulting from both approaches were spatially normalised to the 2.0^3 mm^3 MNI152NLin2009cAsym template downsampled to 3.0^3 mm^3, as was done during the GLM analysis.

Group-level statistical testing was performed for the VB Index maps at each resolution. For each EPI sequence and for each VB Index approach, the average median VB Index across the group was calculated and used as the baseline during the statistical testing. A mass univariate one-sample t-test was applied for each sequence to assess whether voxels had a VB Index higher than the group median VB Index, with an alpha level of 0.05. As with the GLM, Bonferroni correction was applied to control the familywise error rate. Figure 6 provides an illustration of the workflow performed during the analysis of VB Index.

Comparison of statistical maps

The statistical maps of the GLM and VB Index were compared across sequence protocols to assess the consistency of results across sequence protocols. This was achieved using the Dice-Sørensen coefficient (DC) which is defined as the ratio of the intersection between a pair of statistical maps (X and Y) to the to the average number of statistically significant voxels in both statistical maps as shown by equation 1[48]. This procedure was performed for both the statistical maps obtained with the GLM and the VB Index.

$$DC = \frac{2|X \cap Y|}{|X| + |Y|} \tag{1}$$

Cross-comparison of the GLM and VB Index statistical maps were performed using the Overlap coefficient (OC). The Overlap coefficient assesses the ratio of the intersection between the two statistical maps to the total number of statistically significant voxels in the smaller statistical map as given in equation 2[49]. The Dice-Sørensen coefficient was not suitable for the cross-comparison between the VB Index and the GLM, since the results of the VB Index were expected from first principles to be a superset of the results of the GLM. Therefore, the Overlap coefficient assessed the spatial intersection of VB and GLM statistical maps with the GLM statistical maps as reference.

$$OC = \frac{|X \cap Y|}{\min(|X|, |Y|)} \tag{2}$$

Code availability

The code used during the study is available on Github:
https://github.com/KristianGalea/VB-Pulse-Sequence-Evaluation.git

References

1. Wu, T. *et al.* Regional homogeneity changes in patients with Parkinson's disease. *Hum. Brain Mapp.* **30**, 1502–1510, DOI: 10.1002/hbm.20622 (2009).
2. Xu, Z. *et al.* Regional homogeneity and functional connectivity analysis of resting-state magnetic resonance in patients with bipolar II disorder. *Medicine* **98**, e17962, DOI: 10.1097/MD.0000000000017962 (2019).
3. Bajada, C. J. *et al.* A tutorial and tool for exploring feature similarity gradients with MRI data. *NeuroImage* **221**, 117140, DOI: 10.1016/j.neuroimage.2020.117140 (2020).
4. Farrugia, C., Galdi, P., Irazu, I. A., Scerri, K. & Bajada, C. J. Local gradient analysis of human brain function using the Vogt-Bailey Index. *Brain Struct. Funct.* **229**, 497–512, DOI: 10.1007/s00429-023-02751-7 (2024).
5. Gountouna, V.-E. *et al.* Functional Magnetic Resonance Imaging (fMRI) reproducibility and variance components across visits and scanning sites with a finger tapping task. *NeuroImage* **49**, 552–560, DOI: 10.1016/j.neuroimage.2009.07.026 (2010).
6. Witt, S. T., Laird, A. R. & Meyerand, M. E. Functional neuroimaging correlates of finger-tapping task variations: an ALE meta-analysis. *NeuroImage* **42**, 343–356, DOI: 10.1016/j.neuroimage.2008.04.025 (2008).
7. Turesky, T. K., Olulade, O. A., Luetje, M. M. & Eden, G. F. An fMRI study of finger tapping in children and adults. *Hum. Brain Mapp.* **39**, 3203–3215, DOI: 10.1002/hbm.24070 (2018).
8. Wüthrich, F. *et al.* Test–retest reliability of a finger-tapping fMRI task in a healthy population. *Eur. J. Neurosci.* **57**, 78–90, DOI: 10.1111/ejn.15865 (2023).
9. Friston, K. J. *et al.* Statistical parametric maps in functional imaging: A general linear approach. *Hum. Brain Mapp.* **2**, 189–210, DOI: 10.1002/hbm.460020402 (1994).
10. Poline, J.-B. & Brett, M. The general linear model and fMRI: Does love last forever? *NeuroImage* **62**, 871–880, DOI: 10.1016/j.neuroimage.2012.01.133 (2012).
11. Leibovici, D. G. & Smith, S. Comparing groups of subjects in fMRI studies: a review of the GLM approach. (2001).
12. Monti, M. M. Statistical Analysis of fMRI Time-Series: A Critical Review of the GLM Approach. *Front. Hum. Neurosci.* **5**, DOI: 10.3389/fnhum.2011.00028 (2011).
13. Zang, Y., Jiang, T., Lu, Y., He, Y. & Tian, L. Regional homogeneity approach to fMRI data analysis. *NeuroImage* **22**, 394–400, DOI: 10.1016/j.neuroimage.2003.12.030 (2004).
14. Lv, Y., Margulies, D. S., Villringer, A. & Zang, Y.-F. Effects of Finger Tapping Frequency on Regional Homogeneity of Sensorimotor Cortex. *PLOS ONE* **8**, e64115, DOI: 10.1371/journal.pone.0064115 (2013). Publisher: Public Library of Science.
15. Triantafyllou, C. *et al.* Comparison of physiological noise at 1.5 T, 3 T and 7 T and optimization of fMRI acquisition parameters. *NeuroImage* **26**, 243–250, DOI: 10.1016/j.neuroimage.2005.01.007 (2005).
16. Wilson, S. M., Bautista, A., Yen, M., Lauderdale, S. & Eriksson, D. K. Validity and reliability of four language mapping paradigms. *NeuroImage: Clin.* **16**, 399–408, DOI: 10.1016/j.nicl.2016.03.015 (2017).
17. Pimentel, M. A. F., Vilela, P., Sousa, I. & Figueiredo, P. Localization of the hand motor area by arterial spin labeling and blood oxygen level-dependent functional magnetic resonance imaging. *Hum. Brain Mapp.* **34**, 96–108, DOI: 10.1002/hbm.21418 (2011).
18. Thiebaut de Schotten, M., Urbanski, M., Valabregue, R., Bayle, D. J. & Volle, E. Subdivision of the occipital lobes: An anatomical and functional MRI connectivity study. *Cortex* **56**, 121–137, DOI: 10.1016/j.cortex.2012.12.007 (2014).
19. Weibull, A., Gustavsson, H., Mattsson, S. & Svensson, J. Investigation of spatial resolution, partial volume effects and smoothing in functional MRI using artificial 3D time series. *NeuroImage* **41**, 346–353, DOI: 10.1016/j.neuroimage.2008.02.015 (2008).
20. Lotze, M. *et al.* fMRI Evaluation of Somatotopic Representation in Human Primary Motor Cortex. *NeuroImage* **11**, 473–481, DOI: 10.1006/nimg.2000.0556 (2000).

21. Beisteiner, R. *et al.* Finger Somatotopy in Human Motor Cortex. *NeuroImage* **13**, 1016–1026, DOI: 10.1006/nimg.2000.0737 (2001).

22. Dechent, P. & Frahm, J. Functional somatotopy of finger representations in human primary motor cortex. *Hum. Brain Mapp.* **18**, 272–283, DOI: 10.1002/hbm.10084 (2003). _eprint: https://onlinelibrary.wiley.com/doi/pdf/10.1002/hbm.10084.

23. Peirce, J. *et al.* PsychoPy2: Experiments in behavior made easy. *Behav. Res. Methods* **51**, 195–203, DOI: 10.3758/s13428-018-01193-y (2019).

24. Gorgolewski, K. J. *et al.* The brain imaging data structure, a format for organizing and describing outputs of neuroimaging experiments. *Sci. Data* **3**, 160044, DOI: 10.1038/sdata.2016.44 (2016). Publisher: Nature Publishing Group.

25. Esteban, O. *et al.* fMRIPrep: a robust preprocessing pipeline for functional MRI. *Nat. Methods* **16**, 111–116, DOI: 10.1038/s41592-018-0235-4 (2019).

26. Esteban, O. *et al.* Analysis of task-based functional MRI data preprocessed with fMRIPrep. *Nat. protocols* **15**, 2186–2202, DOI: 10.1038/s41596-020-0327-3 (2020).

27. Woolrich, M. W. *et al.* Bayesian analysis of neuroimaging data in FSL. *NeuroImage* **45**, S173–S186, DOI: 10.1016/j.neuroimage.2008.10.055 (2009).

28. Smith, S. M. *et al.* Advances in functional and structural MR image analysis and implementation as FSL. *NeuroImage* **23 Suppl 1**, S208–219, DOI: 10.1016/j.neuroimage.2004.07.051 (2004).

29. Jenkinson, M., Beckmann, C. F., Behrens, T. E. J., Woolrich, M. W. & Smith, S. M. FSL. *NeuroImage* **62**, 782–790, DOI: 10.1016/j.neuroimage.2011.09.015 (2012).

30. Tustison, N. J. *et al.* N4ITK: improved N3 bias correction. *IEEE transactions on medical imaging* **29**, 1310–1320, DOI: 10.1109/TMI.2010.2046908 (2010).

31. Avants, B. B. *et al.* A reproducible evaluation of ANTs similarity metric performance in brain image registration. *NeuroImage* **54**, 2033–2044, DOI: 10.1016/j.neuroimage.2010.09.025 (2011).

32. Fischl, B. FreeSurfer. *NeuroImage* **62**, 774–781, DOI: 10.1016/j.neuroimage.2012.01.021 (2012).

33. Klein, A. *et al.* Mindboggling morphometry of human brains. *PLOS Comput. Biol.* **13**, e1005350, DOI: 10.1371/journal.pcbi.1005350 (2017). Publisher: Public Library of Science.

34. Tustison, N. J. *et al.* The ANTsX ecosystem for quantitative biological and medical imaging. *Sci. Reports* **11**, 9068, DOI: 10.1038/s41598-021-87564-6 (2021). Publisher: Nature Publishing Group.

35. Ciric, R. *et al.* TemplateFlow: FAIR-sharing of multi-scale, multi-species brain models. *Nat. Methods* **19**, 1568–1571, DOI: 10.1038/s41592-022-01681-2 (2022).

36. Fonov, V., Evans, A., McKinstry, R., Almli, C. & Collins, D. Unbiased nonlinear average age-appropriate brain templates from birth to adulthood. *NeuroImage* **47**, S102, DOI: 10.1016/S1053-8119(09)70884-5 (2009).

37. Fonov, V. *et al.* Unbiased average age-appropriate atlases for pediatric studies. *NeuroImage* **54**, 313–327, DOI: 10.1016/j.neuroimage.2010.07.033 (2011).

38. Jenkinson, M., Bannister, P., Brady, M. & Smith, S. Improved Optimization for the Robust and Accurate Linear Registration and Motion Correction of Brain Images. *NeuroImage* **17**, 825–841, DOI: 10.1006/nimg.2002.1132 (2002).

39. Greve, D. N. & Fischl, B. Accurate and robust brain image alignment using boundary-based registration. *NeuroImage* **48**, 63–72, DOI: 10.1016/j.neuroimage.2009.06.060 (2009).

40. Power, J. D., Barnes, K. A., Snyder, A. Z., Schlaggar, B. L. & Petersen, S. E. Spurious but systematic correlations in functional connectivity MRI networks arise from subject motion. *NeuroImage* **59**, 2142–2154, DOI: 10.1016/j.neuroimage.2011.10.018 (2012).

41. Behzadi, Y., Restom, K., Liau, J. & Liu, T. T. A component based noise correction method (CompCor) for BOLD and perfusion based fMRI. *NeuroImage* **37**, 90–101, DOI: 10.1016/j.neuroimage.2007.04.042 (2007).

42. Patriat, R., Reynolds, R. C. & Birn, R. M. An improved model of motion-related signal changes in fMRI. *NeuroImage* **144**, 74–82, DOI: 10.1016/j.neuroimage.2016.08.051 (2017).

43. Alahmadi, A. A. S. Effects of different smoothing on global and regional resting functional connectivity. *Neuroradiology* **63**, 99–109, DOI: 10.1007/s00234-020-02523-8 (2021).

44. Glover, G. H. Deconvolution of Impulse Response in Event-Related BOLD fMRI1. *NeuroImage* **9**, 416–429, DOI: 10.1006/nimg.1998.0419 (1999).

45. Parkes, L., Fulcher, B., Yücel, M. & Fornito, A. An evaluation of the efficacy, reliability, and sensitivity of motion correction strategies for resting-state functional MRI. *NeuroImage* **171**, 415–436, DOI: 10.1016/j.neuroimage.2017.12.073 (2018).

46. Satterthwaite, T. D. *et al.* An improved framework for confound regression and filtering for control of motion artifact in the preprocessing of resting-state functional connectivity data. *NeuroImage* **64**, 240–256, DOI: 10.1016/j.neuroimage.2012.08.052 (2013).

47. Kliemann, D. *et al.* Caltech Conte Center, a multimodal data resource for exploring social cognition and decision-making. *Sci. Data* **9**, 138, DOI: 10.1038/s41597-022-01171-2 (2022).

48. Bach, P. *et al.* Reliability of the fMRI-based assessment of self-evaluation in individuals with internet gaming disorder. *Eur. Arch. Psychiatry Clin. Neurosci.* **272**, 1119–1134, DOI: 10.1007/s00406-021-01307-2 (2022).

49. Alarcon, N. Similarity in graphs: Jaccard versus the Overlap Coefficient (2019).

Acknowledgements

The authors would like to thank the University of Malta's MRI Platform (UMRI) for access to scanning equipment and services, use of its infrastructure, and resources such as documentation and preprocessing scripts. Furthermore, the authors would also like to acknowledge that the study is part of the Enhancing Astronaut Neuro-Imaging Capabilities: Toolbox Optimization & Modification (Operation TOM) Project, financed by Xjenza Malta through the Space Upstream Programme 2023 (grant no. SUP-2023-01). . RS is supported by fellowship funding from the National Imaging Facility (NIF), an Australian Government National Collaborative Research Infrastructure Strategy (NCRIS) capability.

Author contributions statement

C.J.B. devised the idea for the study. K.G., and A.A.E. performed the data analyses. K.G., L.B., C.J.B. and P.G. wrote the manuscript. All authors reviewed and edited multiple drafts of the manuscript.

Additional information

Competing interests

The authors declare no competing interests.

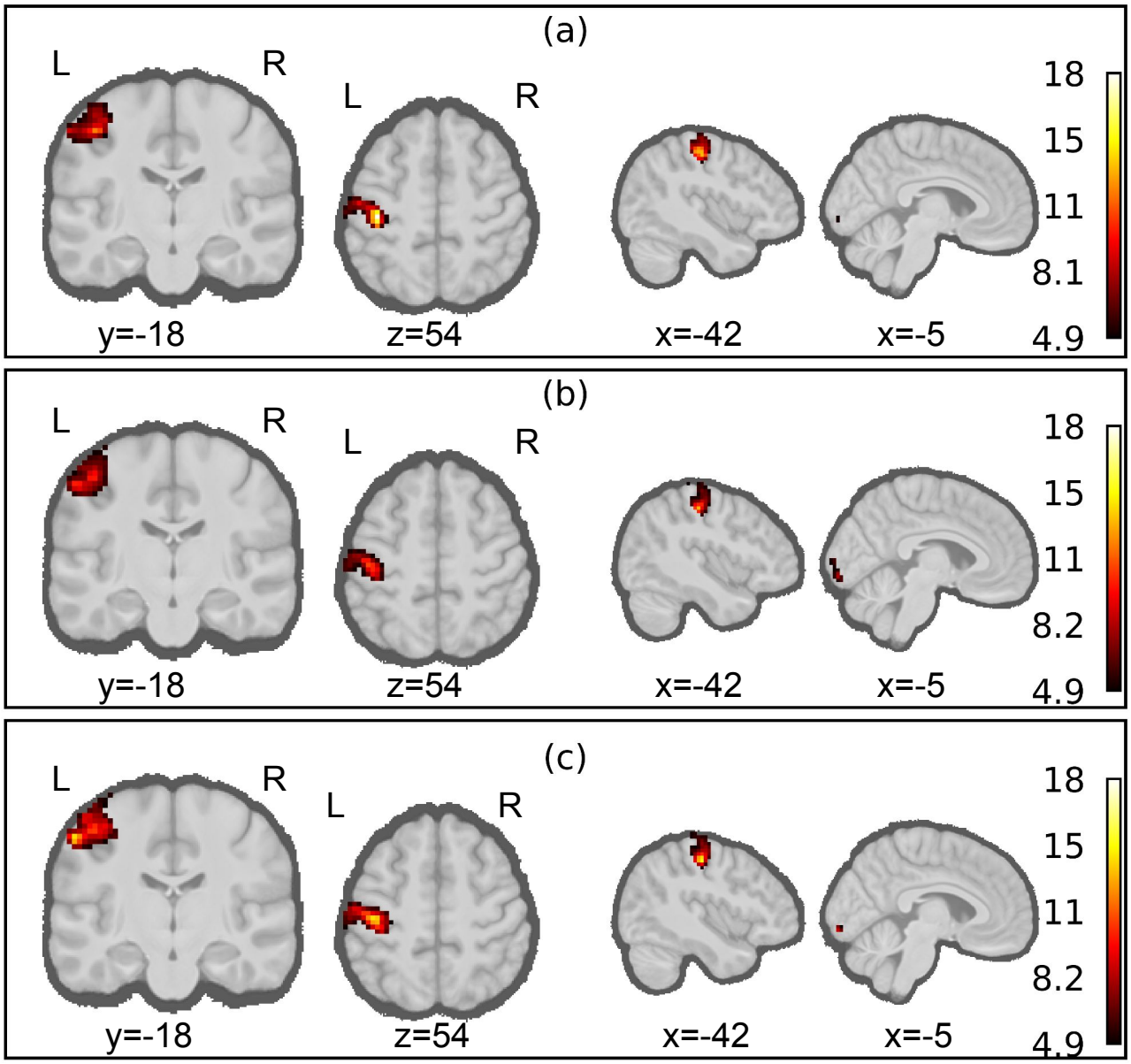

Figure 1. Bonferroni thresholded ($p<0.05$) GLM statistical t-maps. The second-level statistical maps are overlaid on the group average T1-weighted image spatially normalised to the MNI152NLin2009cAsym template. The first row (a), second row (b) and third row (c) displays the t-maps from the 1.8^3 mm^3, 2.0^3 mm^3, and 2.5^3 mm^3 sequences respectively.

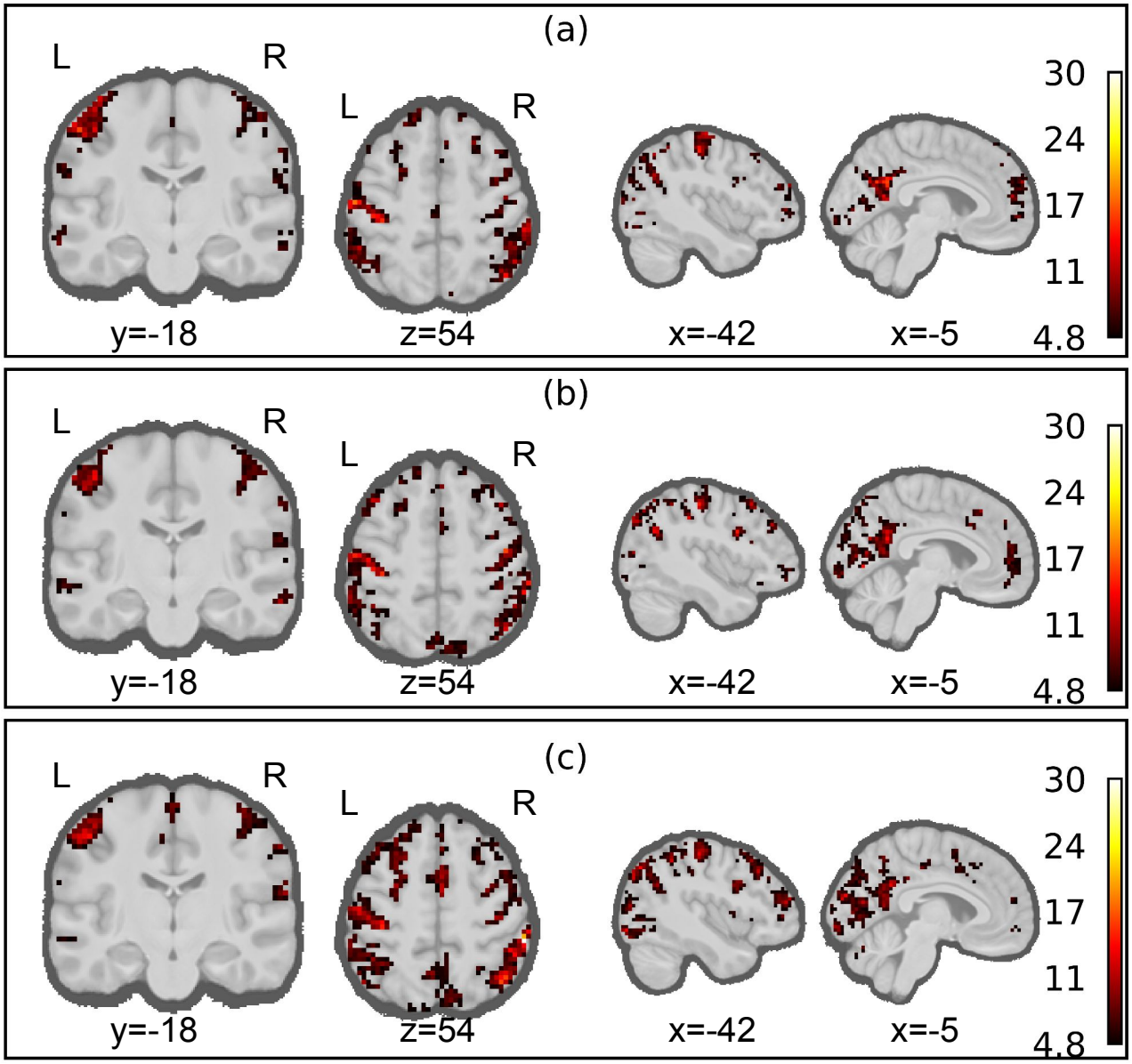

Figure 2. Bonferroni thresholded ($p<0.05$) statistical t-maps obtained with VB1. The first row (a), second row (b), and third row (c) display the statistical maps obtained with the 1.8^3 mm^3, 2.0^3 mm^3, and 2.5^3 mm^3 sequences respectively.

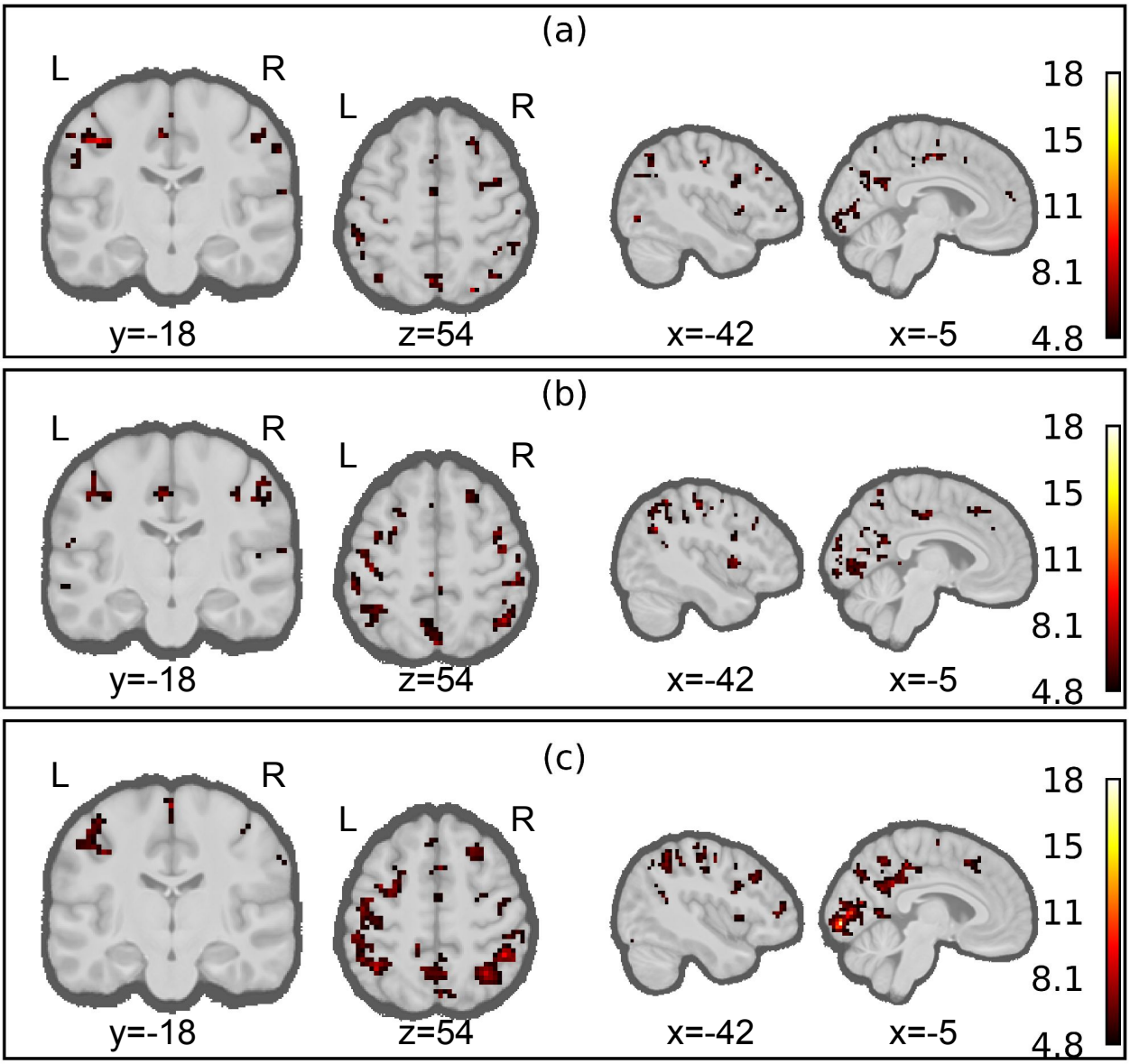

Figure 3. Bonferroni thresholded ($p<0.05$) statistical t-maps obtained with VB2. The first row (a), second row (b), and third row (c) display the statistical maps obtained with the 1.8^3 mm^3, 2.0^3 mm^3, and 2.5^3 mm^3 sequences respectively.

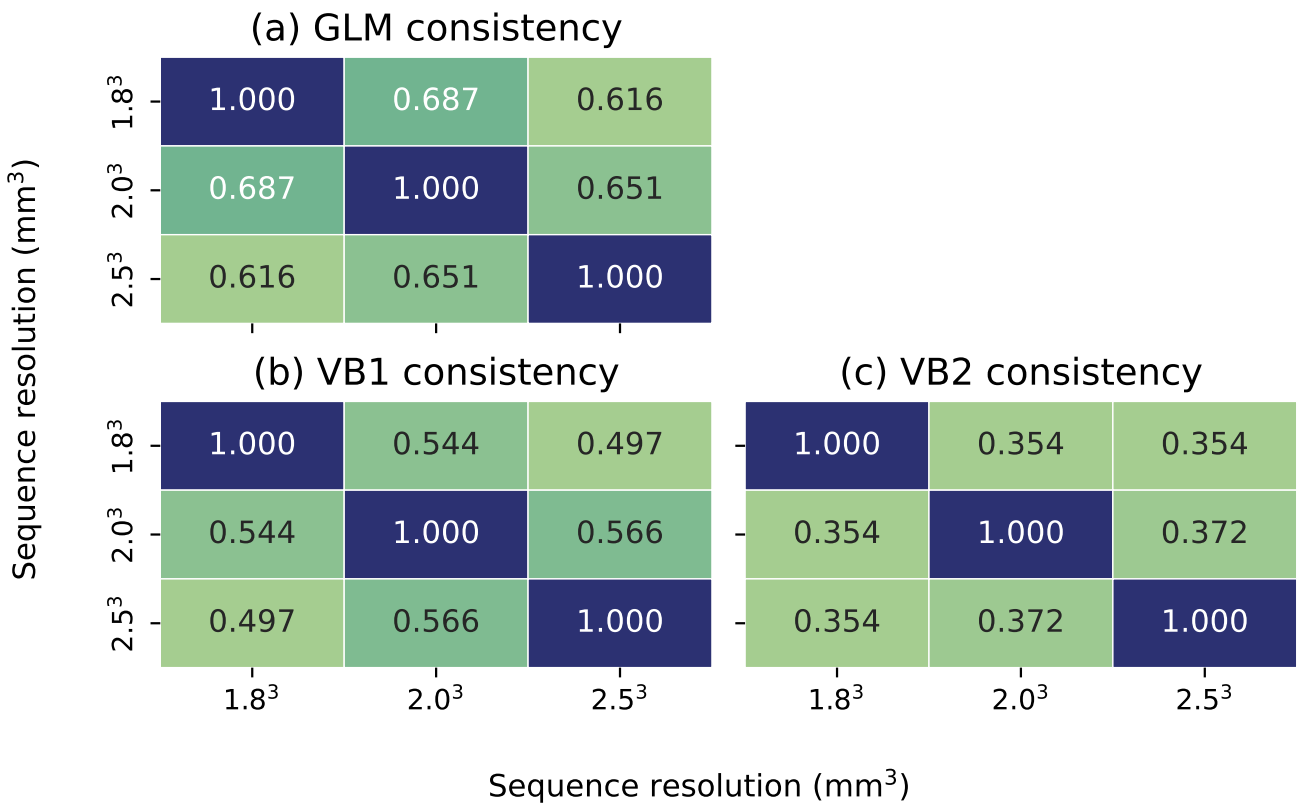

Figure 4. The Dice coefficients are shown as symmetric matrices, quantifying the consistency of results across pulse sequences. a) quantifies the GLM, b) VB1, and c) VB2.

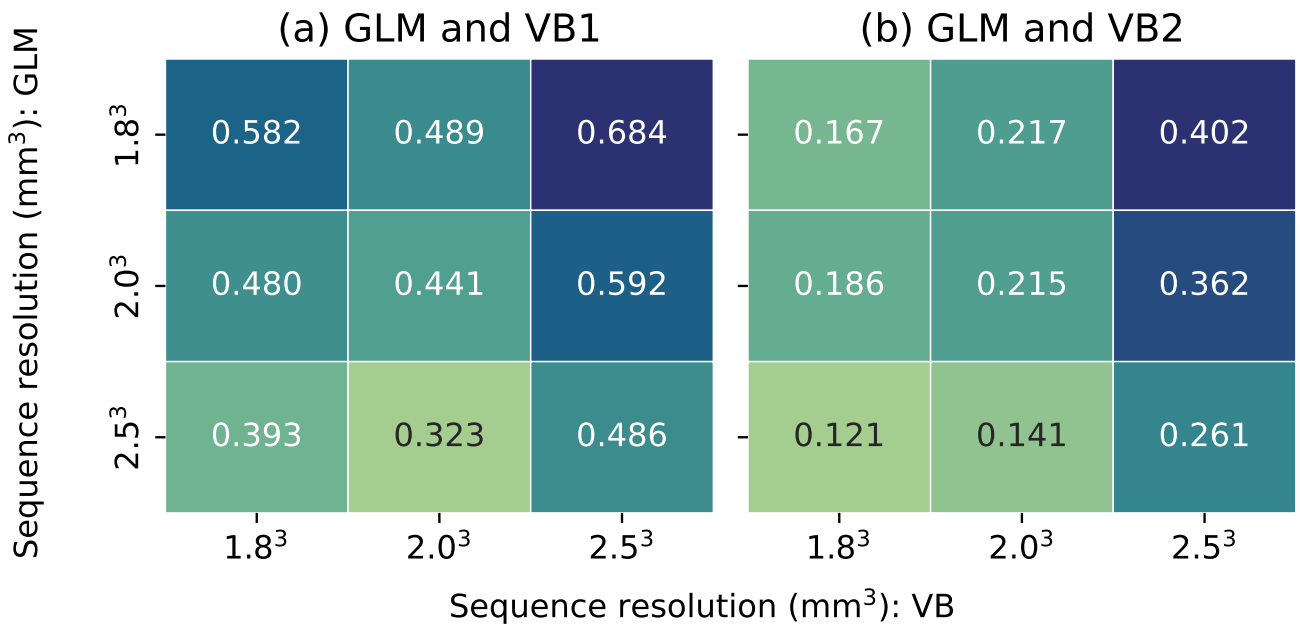

Figure 5. The Overlap coefficients showing the overlap between the GLM and a) VB1, b) VB2 across sequences.

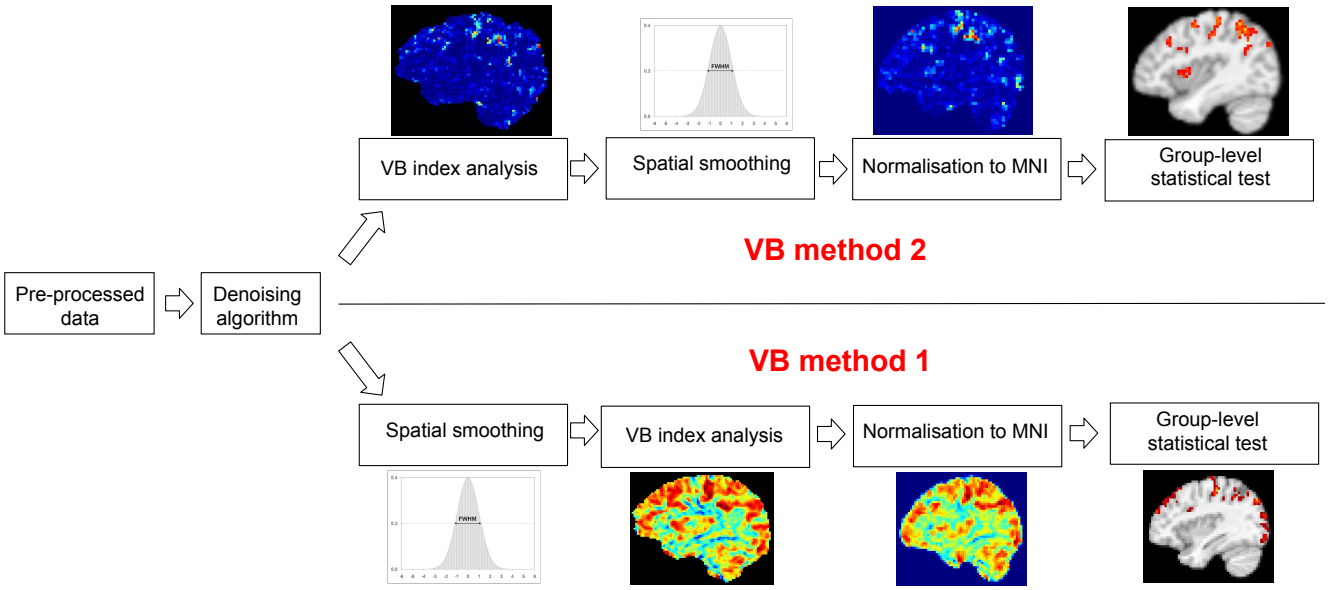

Figure 6. The workflow of the VB method 1 and VB method 2.